Analysis of the Optimal Mass Problem for Aerobraking Tethers

Steven G. Tragesser,* James M. Longuski,† Jordi Puig-Suari‡ and John P. Mechalas*
Purdue University, West Lafayette, IN 47907-1282

Abstract

Earlier work has demonstrated the feasibility of using aerobraking tethers for solar system exploration. Numerical optimization techniques have been used to determine the minimum tether mass required for aerobraking maneuvers at all atmosphere-bearing bodies in the solar system. The results indicate that in all cases, the mass of the tether is significantly lower that the propellant mass required for the maneuver. However, the nonlinear programming techniques used to solve the optimization problem cannot be used to prove that the solution obtained is a global minimum for the problem; it is only guaranteed to be a local minimum. In this paper, techniques are developed to determine if, in fact, a given solution is a global minimum. The minimum tether mass maneuvers obtained previously are shown to be global minima.

1 Introduction

Previous work by Puig-Suari and Longuski [1] demonstrates the physical feasibility of the aerobraking tether concept. This system consists of an orbiter and a probe connected by a thin tether (see Fig.1). When the spacecraft arrives at a planet, the probe travels through the atmosphere and aerodynamic forces provide the change in velocity required to capture the vehicle into orbit around the planet, thus, eliminating the need for chemical rockets. During the maneuver, the orbiter remains outside the sensible atmosphere and requires no aerodynamic shielding. In order to maximize the orbiter's altitude (clearance) above the probe, a *vertical dumbbell maneuver* is used in which the tether achieves a vertical orientation at closest approach ($\alpha = \alpha_{min} = 0$). The fly-through orientation of the tether in this maneuver produces large aerodynamic torques on the vehicle which tend to spin the tether and plunge the orbiter into the atmosphere, but this effect can be eliminated by spinning the tether in the opposite direction during approach. In [2] this maneuver is used to compare the performance of the aerobraking tether to that of traditional propulsion systems in missions to all the atmosphere-bearing bodies in the solar system. The study assumes Hohmann transfers from Earth and capture into near parabolic orbit ($e < 1$) at the destination planet. The tether material is assumed to be Hercules AS4 graphite with an ultimate strength, σ, of $3.6\,GN/m^2$ and a density, ρ, of $1800\,kg/m^3$. A propellant with an I_{sp} of $300\,s$ is used for comparison to chemical rockets. The relative performance of the two systems is determined by comparing the mass of the tether and the mass of the propellant required to capture the orbiter. The results indicate that, in all cases, the aerobraking tether is superior to chemical rockets. The maneuvers and tethered systems developed in [2] are used as baselines for subsequent studies. For example, the system designed for Mars has the following characteristics:

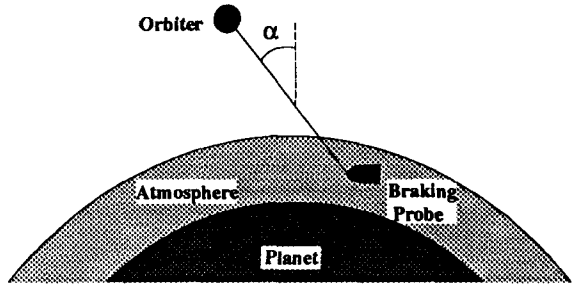

Fig. 1. Aerobraking Tether

Tether length (l_t):	$14.5\,km$
Tether diameter (d):	$2.34\,mm$
Tether mass (m_t):	$112\,kg$
Probe area (S_p):	$605\,m^2$

(1)

*Graduate Student, School of Aeronautics and Astronautics.

†Associate Professor, School of Aeronautics and Astronautics. Associate Fellow AIAA. Member AAS.

‡Visiting Assistant Professor, School of Aeronautics and Astronautics, Member AIAA.

Copyright © 1994 by S. G. Tragesser, J. M. Longuski, J. Puig-Suari and J. P. Mechalas. Published by the American Institute of Aeronautics and Astronautics, Inc. with permission.

and will be referred to as the *design tether* in this paper.

The analysis in [2] proves the mass advantage of the aerobraking tether, but studies only vertical dumbbell maneuvers. The work in [3] focuses on determining the maneuver which provides the minimum tether mass. No explicit formula for the cost function is available for the aerobraking tether and, so, nonlinear programming techniques are required to solve the problem. The use of these techniques on the aerobraking tether problem is very demanding computationally, since every function evaluation requires the numerical simulation of a complete aerobraking maneuver. For this reason the analysis in [3] as well as in this paper models the tether as a rigid rod with distributed gravitational and aerodynamic forces. Note, however, that the rigid rod model provides very accurate results when compared with more realistic flexible tether models developed in [4,5]. In general, any tether aerobraking maneuver can be defined by the orientation and angular velocity of the system outside the atmosphere, α_0 and $\dot{\alpha}_0$ respectively, and the radius of the orbit at periapsis, r_{per}. In addition, the dimensions of the tether may vary during the optimization. However, the minimum mass is found by making the tether just thick enough to withstand the forces encountered during a particular maneuver. Therefore, only the length of the tether is required as a search variable. In addition, some constraints must be included to guarantee that the resulting optimum maneuver is acceptable. First, the final eccentricity after the maneuver, e_f, must be equal to the eccentricity of the target orbit, e_c, which is included as an equality constraint. Next, an inequality constraint is introduced to ensure that the orbiter's clearance above the probe, Δh, is greater than a set minimum, Δh_c. Finally, a second inequality constraint eliminates any maneuver in which compressive forces occur by requiring the minimum tension on the tether, T_{min}, to be positive. Note that compressive forces (negative tension) can be present since the tether is modeled as a rigid rod. Mathematically the problem can be written as:

$$\begin{aligned} \text{Minimize:} \quad & m_t(x) \\ & x = [l_t, \alpha_0, \dot{\alpha}_0, r_{per}]^T \end{aligned} \tag{2}$$

$$\begin{aligned} \text{subject to:} \quad & e_f - e_c = 0 \\ & \Delta h - \Delta h_c > 0 \\ & T_{min} > 0 \end{aligned} \tag{3}$$

This problem is very complex, but we can obtain some insight into the behavior of the system by solving a simpler, related case: the minimum force problem. In this case the tether dimensions are fixed and the optimization algorithm searches for the maneuver which provides the lowest maximum force on the tether, F_{max}, for the given constraints. Mathematically:

$$\begin{aligned} \text{Minimize:} \quad & F_{max}(x) \\ & x = [\alpha_0, \dot{\alpha}_0, r_{per}]^T \end{aligned} \tag{4}$$

subject to constraints (3).

In [3] the minimum force problem is solved at Mars using the design tether, a zero clearance constraint, and several target eccentricities (i.e., ΔV's). The zero clearance constraint allows for the possibility of widely varying fly-through maneuvers (including a horizontal maneuver known as a *drag-chute maneuver* [6]) The results are shown in Table 1 and indicate that the vertical dumbbell is the minimum force maneuver only when low ΔV's are required (which corresponds to high final eccentricity). In all other cases the tethered system has some inclination during fly through ($\alpha_{min} > 0$), and these are referred to as *inclined maneuvers*. The characteristics of these maneuvers are very different from those of the original vertical dumbbell maneuver. Figure 2 shows the tether forces on the probe for the near parabolic capture ($e_f = 0.9999$) in Table 1, an inclined solution with $\alpha_{min} = 55°$. Initially, outside the atmosphere, small tension forces are present due to the spin of the system. Once the spacecraft enters the atmosphere, aerodynamic effects produce large tension forces, and the maximum forces occur in this portion of the trajectory. Finally, the system exits the atmosphere and only small spin tension remains. This behavior is completely different from that of a vertical dumbbell maneuver. Figure 3 shows the tether forces for the $e_f = 1.5$ maneuver in Table 1, a vertical dumbbell. Here the maximum forces on the system occur outside the atmosphere and are due to the spin of the system. During fly through, the spin rate goes to zero and so does the tension on the tether, since, due to the vertical orientation of the system, aerodynamic forces act in a direction normal to the tether and produce no tension. Although this case does not result in aerocapture at Mars, we know that similar behavior is exhibited during aerocapture at other planets (e.g., Jupiter, Table 2).

Next, the analysis in [3] uses a nonlinear programming algorithm to solve the optimal mass maneuver for all atmosphere-bearing bodies in the solar system. The assumptions made in [2] and mentioned above are also applied in this case. The final results are shown in Table 2. Note that both types of maneuvers, vertical and inclined, are represented. The inclined maneuvers achieve a significant reduction in tether mass with respect to the vertical dumbbell ma-

Table 1. Mars Minimum Force Results ($l_t = 14.5\,km$, $\Delta h_c = 0km$)

e_f	$\Delta V(km/s)$	$\Delta h(km)$	$F_{max}(N)$	$\alpha_{min}(deg)$	Maneuver Type
0.9999	0.676	8.21	6990	55.3	I (Inclined)
1.2000	0.422	11.2	3950	39.2	I (Inclined)
1.5000	0.0819	14.5	249	-0.660	V (Vertical)

Table 2. Aerocapture Results for Solar System Exploration (Optimal Mass)

Values	Venus	Earth	Mars	Jupiter	Saturn	Uranus	Neptune	Titan
$\Delta V(km/s)$	0.35	0.39	0.67	0.27	0.41	0.50	0.34	1.31
Propellant Mass (kg)	126	142	256	96	149	185	122	559
Tether Mass (kg)	25.9	30.5	66.4	18.8	44.1	67.2	32.6	282
Savings (%)	79%	79%	74%	80%	70%	64%	73%	50%
Savings (kg)	99.1	112	190	77.2	105	118	89	277
Length (km)	12.4	10.5	20.7	36.1	54.4	72.7	72.8	112
Diameter (mm)	1.22	1.43	1.51	0.607	0.757	0.809	0.563	1.33
Probe Area (m^2)	999	818	605	2370	1910	1810	2670	747
Maximum Force (N)	4180	5820	6420	1050	1630	1850	899	5030
Minimum $\alpha(deg)$	27.7	28.4	45.4	0.46	0.18	0.27	0.75	41.0
Maneuver Type	I	I	I	V	V	V	V	I

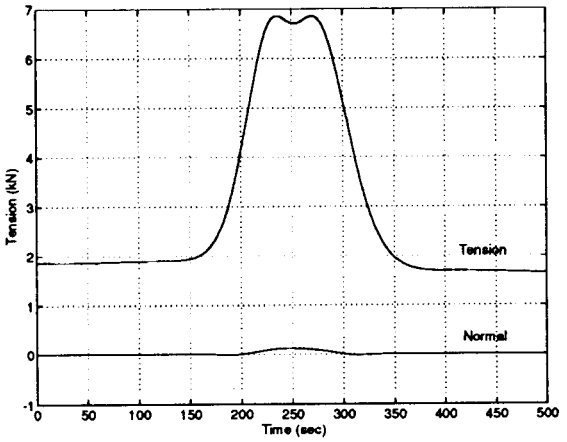

Fig. 2. Tether Forces: Inclined Maneuver ($e_f = 0.9999$)

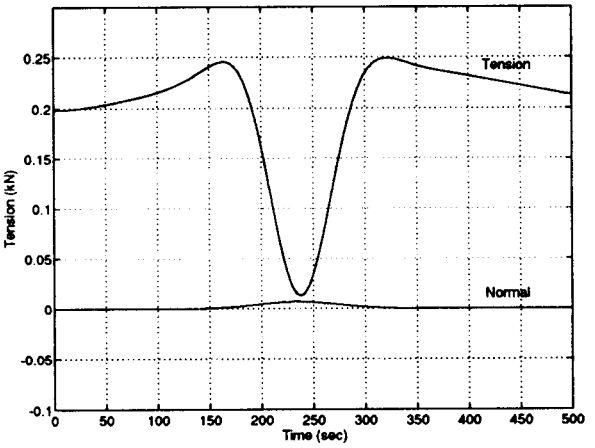

Fig. 3. Tether Forces: Vertical-Dumbbell Maneuver ($e_f = 1.5$)

neuvers in [2]. These maneuvers are known to be local minima for the tether mass. However, since they are obtained numerically there is no guarantee that they are global minima. The purpose of the work presented in this paper is to determine if the previously found solutions are global minima or if even better aerobraking tether maneuvers are possible.

2 Minimum Force Problem

As a preliminary step in investigating whether the minimum mass solutions are global, we investigate the simpler problem of minimizing the maximum force on the tether, F_{max}. As mentioned previously, this is a three-parameter system (α_0, $\dot{\alpha}_0$, r_{per}).

The number of variables of this system can be decreased from three to two by enforcing the eccentricity constraint in (3):

$$f(x) = e_f - e_c = 0 \tag{5}$$

Thus, *all* maneuvers that achieve a desired eccentricity can be graphically illustrated in two dimensions. This is accomplished by fixing two of the state variables so that $f(x)$ in Equation (5) becomes a scalar-valued function which can then be solved for the third (free) variable. We use a root finder to solve constraint (5) for r_{per} for sets of values of α_0 and $\dot{\alpha}_0$. For instance, (in the case of Mars), if we choose an initial orientation of 180^o and an initial angular velocity of $0.005\ rad/s$, then solving for the target periapsis yields an altitude of $83.41\ km$ for $e_f = 0.9999$. Intuitively, we know $f(x)$ has a unique solution because flying through lower altitudes for a given orientation and spin rate will always lower final eccentricity while flying higher will decrease the braking effect. Thus, the solution for r_{per} is unique for given α_0 and $\dot{\alpha}_0$.

Once the state resulting in the desired final eccentricity is found, information about the maneuver such as the maximum and minimum forces on the tether, the minimum orientation angle, α_{min}, and the difference in minimum altitude of the orbiter and probe (the clearance), Δh, can be determined. Fig. 4 shows the force contours of aerobraking maneuvers at Mars which achieve a final eccentricity of $e_f = 0.9999$. We note that there are several local minima and that there are large variations in the force gradient. In order to eliminate unacceptable maneuvers, we enfore the inequality constraints in (3) for clearance and tether compression.

Violating either of these two constraints yields an infeasible maneuver. (Low clearance causes significant aerodynamic forces on the orbiter; compression produces catastrophic bending in the tether.) In order to study a wide range of maneuvers, including the drag chute as the limiting case, we set Δh_c to zero.

The shaded areas in Fig. 4 correspond to maneuvers which violate the inequality constraints. We can now make two important observations about the solution space. First of all, there is an enclosed area that contains *all the acceptable solutions* (Region I). Solutions for values of $\dot{\alpha}_0$ that are not shown all violate one or both of the constraints or are deemed unacceptable because of very high tension. Clearly, initial spin rates much greater than that of the vertical dumbbell maneuver will never outperform the vertical dumbbell (where maximum force is governed by spin rate). Thus, lower upper and upper lower bounds can be established based on the $\pm\dot{\alpha}_0$ corresponding to a vertical dumbbell. Also, if a given initial state vector is a solution, then changing the initial orientation by multiples of 360^o will not change the maneuver. Second, there is only *one minima* in this area of possible solutions (denoted "Optimum Force" on the plot and located at the minimum contour point of $7\,kN$). Therefore, ***this point is the global minimum force for aerocapture at Mars with the design tether.*** Note that this point corresponds to the solution given in Table 1 where $F_{max} = 6990\,N$. Also note that the vertical dumbbell solution [2] is nonoptimal ($F_{max} = 12.7\,kN$) and is located at the edge of the compression constraint.

The task of numerically optimizing the tether forces is not only computationally intensive, but also very prone to problems with robustness. Often, the algorithm becomes trapped in a region in which a constraint is active and, thus, never converges on an acceptable solution. Region II in Fig. 4 is an example of one such region of "no return." The search direction of the algorithm will be towards Region II for initial guesses in the vicinity of Region II, since it contains a *local* minimum force and the exterior penalty method is initially driven by the unconstrained problem. Since there are local minima within this region for the constraint functions as well, it is possible to become trapped at some state in which nearby solutions have an increased force *and* an increased cost due to the constraints.

The planets with vertical dumbbell optimum solutions are most vulnerable to this problem since the vertical dumbbell always borders a region of compressive forces. The problem can be minimized by guessing an initial solution that is near the optimum and increasing the penalty on the constraints.

Region I, on the other hand, is an area in which it is comparatively easy to converge on a minimum. The constraints in this region are inactive and changes in forces are much less sensitive to initial conditions

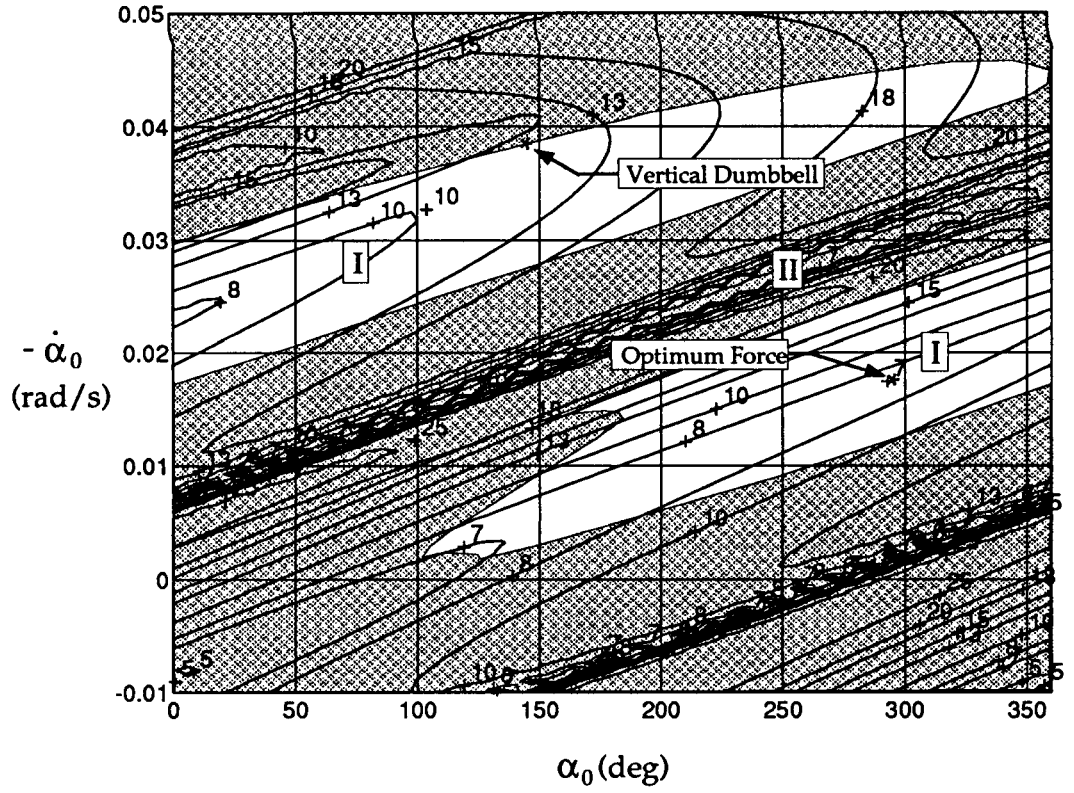

Fig. 4. Mars Forces and Constraints ($e_f = 0.9999$). I.C.'s at $3654km$. Force Contours in kN.

than in Region II. This robustness is a characteristic of the inclined maneuver which may provide advantages in the guidance and control problem.

Next, we investigate the conjecture that ΔV is the primary factor in determining whether the optimum force maneuver is an inclined or vertical dumbbell maneuver. As before, we are interested in showing that there is a unique local minimum in the acceptable region and, thus, it corresponds to the global minimum.

To study the effect of changing the ΔV, we look at cases for Mars with the identical design tether that was used above, but vary the final eccentricity. Fig. 5 shows the case where $e_f = 1.2$. The shape of the force contours is similar to the $e_f = 0.9999$ case, but the magnitudes have dropped due to the decrease in ΔV. The region of feasible solutions (solutions which do not violate the constraints, indicated by the unshaded portion of the plot) is not enclosed in this case. However, solutions for $\dot{\alpha}_0$ that are not shown are rejected because of unacceptably high forces, as before. Therefore, the local minimum shown in Fig. 5 is unique (within the acceptable region) and it is the global minimum for $e_f = 1.2$. Again, the global minimum found in the plot corresponds to the numerical solution in Table 1. For this case, the optimum solution is still an inclined maneuver but its initial conditions and maximum force are much closer to that of the vertical dumbbell than the previous case. Also, the minimum orientation angle is much smaller.

For the $e_f = 1.5$ case, shown in Fig. 6, the minimum force is located just inside the region in which the initial conditions result in compressive forces on the tether. Thus, the unique local minimum in the acceptable region for this case is located on the edge of the infeasible (shaded) area. The resulting optimum force maneuver is then a vertical dumbbell, where the minimum tension on the tether goes to zero. This provides the minimum force in the acceptable region (see Table 1).

These solution space maps clearly indicate that the solutions presented in Table 1 are global. Furthermore, for the range of ΔV's analyzed, there exists only one local minimum in the region containing the acceptable solutions. Note that these ΔV's represent a broad spectrum of maneuver types from a strongly inclined maneuver to a vertical dumbbell, where decreasing the ΔV causes the solution to migrate towards a vertical dumbbell. Since these maneuver types (inclined and vertical dumbbell) have similar characteristics at all the planets, it seems likely that solution space maps at other planets will yield only

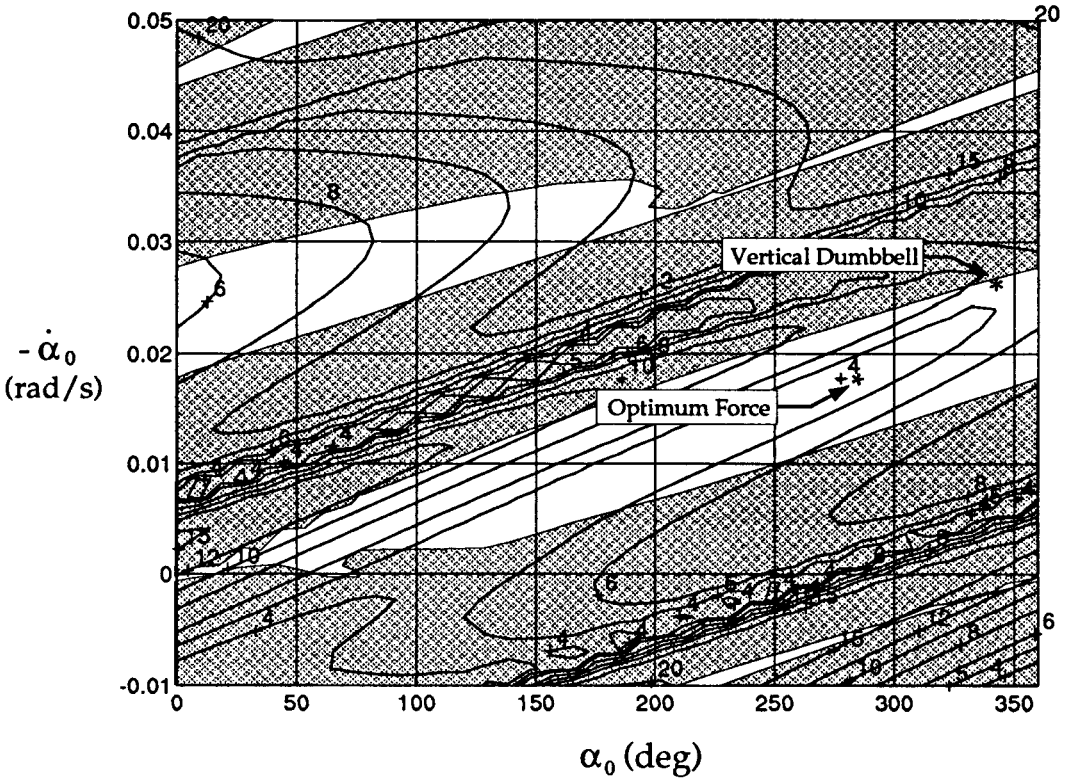

Fig. 5. Mars Forces and Constraints ($e_f = 1.2$). I.C.'s at $3654km$. Force Contours in kN.

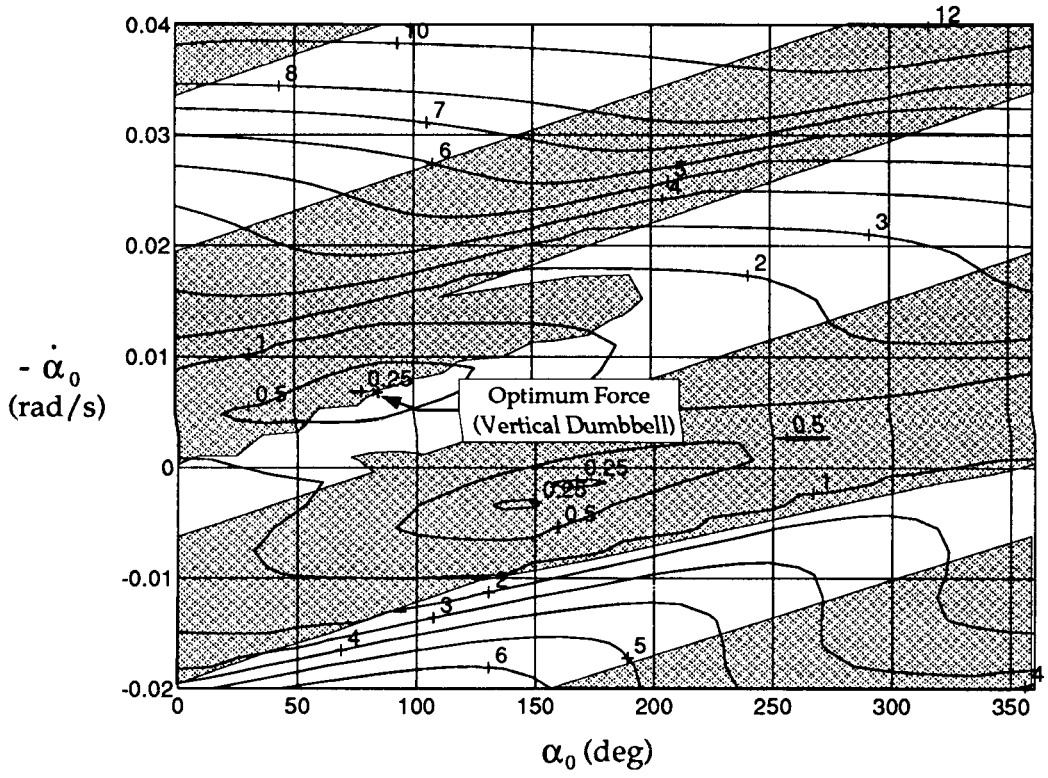

Fig. 6. Mars Forces and Constraints ($e_f = 1.5$). I.C.'s at $3654km$. Force Contours in kN.

one local minimum in the acceptable region. Thus, we conjecture that a local minimum in the acceptable solution space is the global minimum.

3 Extension to Minimum Mass Problem

Several difficulties are encountered when trying to minimize tether mass using the techniques developed to minimize force. Recall that the minimum mass problem is a four-parameter system (l_t, α_0, $\dot{\alpha}_0$, r_{per}). Therefore, fixed values must be independently chosen for three variables now (instead of two for the force analysis) in order to reduce the eccentricity constraint in Equation 5 to a scalar-valued function. A difficulty arises when trying to visually represent the data. A third axis would have to be added to the solution space plots shown above, causing the force contours to become surfaces and the infeasible regions to become solids. Another consequence of this added parameter is a large increase in computational demands which increase with n^3 (as opposed to n^2) where n is the number of points along an axis. For example, generating the minimum force data for Fig. 5 ($n = 35$) takes about 3 hours of CPU time on a sparc 10. Maintaining the same resolution would require more than four days for the minimum mass problem.

These difficulties can be circumvented by changing the clearance constraint in Equations (3) to an equality which reduces the number of variables to two. If we fix the values of α_0 and $\dot{\alpha}_0$ as before, solutions are found by simultaneously solving:

$$\begin{aligned} f_1(\tilde{x}) &= e_f - e_c = 0 \\ f_2(\tilde{x}) &= \Delta h - \Delta h_c = 0 \end{aligned} \tag{6}$$

where

$$\tilde{x} \equiv [l_t, r_{per}]^T \tag{7}$$

Unfortunately, this is still computationally intensive, so we employ an approximate method which uses the data from the minimum force analysis to generate a *derived mass map* which includes the clearance constraint.

With this in mind, for a given point (α_0, $\dot{\alpha}_0$) in the force plot, the tether length that achieves the desired clearance is approximated by

$$l_t = \frac{\Delta h_c}{cos\ \alpha_{min}} \tag{8}$$

Note that if $\Delta h_c = 0$, this implies zero length for all tethers. However, we must emphasize that our goal is to find maneuvers in which the orbiter maintains significant clearance above the probe. For example, in [2], a constant clearance of about 1.8 scale heights (14.5 km for Mars) is assumed. The diameter of the tether can be determined from the maximum force as follows:

$$d = 2\sqrt{\frac{F_{max}}{\sigma\,\pi}} \tag{9}$$

Finally, the mass of the tether is

$$m_t = \rho\, l_t\, \pi\, (d/2)^2 \tag{10}$$

Since α_{min} and F_{max} have already been found in the force analysis, no further simulations are required of the tether equations of motion in order to calculate this approximate mass.

Clearly, the new tether will no longer achieve the prior constraints, and, furthermore, will not be subjected to the same forces. However, all of these objections can be dealt with. First of all, the eccentricity constraint can easily be met by adjusting r_{per}. Secondly, F_{max} and α_{min} are only moderately perturbed. Thus, the first generation derived map represents a first-order approximate solution. It is clear that a second generation (or higher) derived map could be computed, in principle, using a similar procedure, but this leads to further computations. Fortunately, the first generation map achieves the goals of our analysis.

Employing Equations (8) - (10) yields the derived mass map shown in Figures 7-9 which correspond to the minimum force maps shown in Figures 4-6. Note that the unacceptable areas on the plot are shaded. In all three cases, there is only one local minimum in the acceptable region which is denoted as the "derived solution." We have conjectured that the fundamental behavior of the system is retained in the derived mass map. Therefore, the actual system is likely to have only one local (acceptable) minimum. The local minima found numerically in Tables 2 and 3 are then likely candidates for the global optima.

We can now compare the derived solutions with the numerical (local minima) solutions. In Figures 7 and 8, we see a significant difference in $\dot{\alpha}_0$ and α_0, which is not surprising, because large changes in the tether length are necessary for these inclined cases to achieve clearance. Since no length change is necessary for the vertical dumbbell case, Fig. 9 shows very close agreement between the derived and numerical solutions. The fundamental tether characteristics (mass and length) are summarized in Table 3, where we see reasonable agreement in the inclined cases and very close agreement for the vertical dumbbell.

Note that the derived mass map could be improved by using the new tether lengths to calculate the ac tual forces for the target eccentricity as in the minimum force analysis. The F_{max} and α_{min} from this analysis can then be used to estimate a new tether

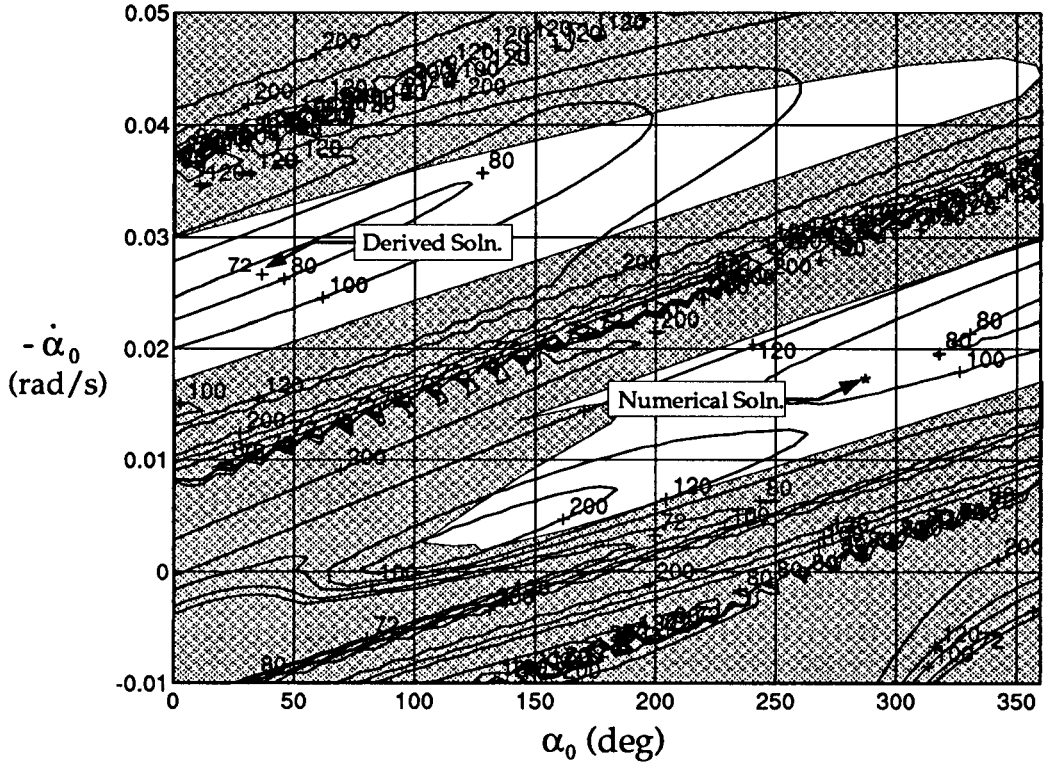

Fig. 7. Derived Masses and Constraints ($e_f = .9999$). I.C.'s at 3654 km. Mass Contours in kg.

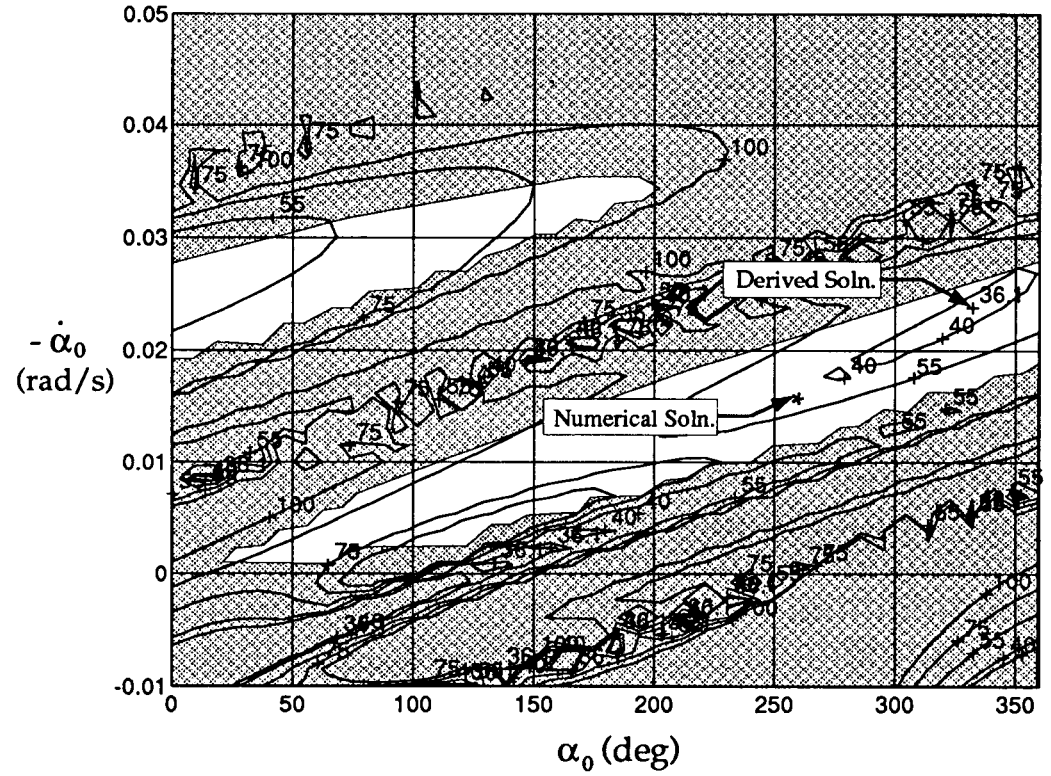

Fig. 8. Derived Masses and Constraints ($e_f = 1.2$). I.C.'s at 3654 km. Mass Contours in kg.

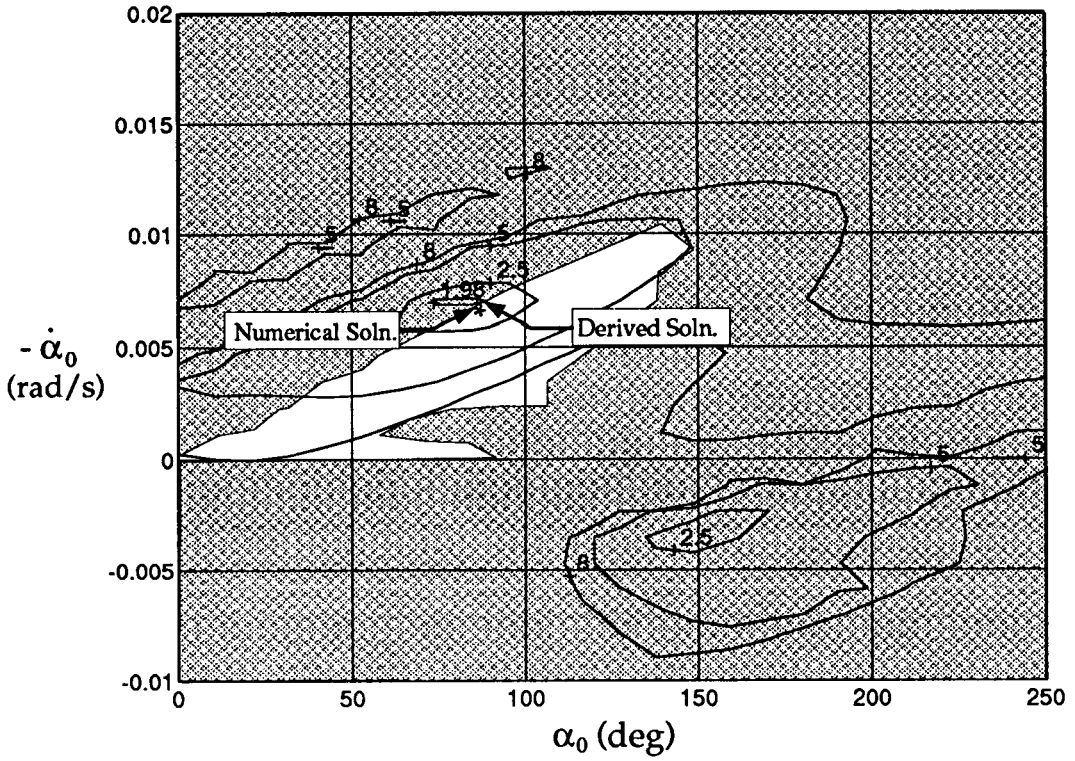

Fig. 9. Derived Masses and Constraints ($e_f = 1.5$). I.C.'s at 3654 km. Mass Contours in kg.

length that would achieve the desired clearance. Iterating over the length and target periapsis in this fashion will eventually yield a solution that satisfies constraints (6), but it is computationally intensive.

Table 3. Mars Minimum Mass Results ($\Delta h_c = 14.5\,km$)

e_f	$\alpha_{min}(deg)$	$F_{max}(kN)$	$l_t(km)$	$m_t(kg)$
1.0	45 (36)[a]	6.4 (8.3)	21 (18)	66 (72)
1.2	34 (20)	3.6 (4.9)	18 (15)	33 (36)
1.5	3.8 (-1)	.25 (.25)	15 (15)	1.8 (2.0)

[a] Parentheses denote derived map results.

4 Conclusion

The local minimum force and mass solutions obtained previously for the aerobraking tether appear to be global optima. An exhaustive search reveals no new type of tether aerobraking maneuver; therefore, the optima consist of vertical dumbbell maneuvers and inclined maneuvers.

5 Acknowledgements

Part of this work was supported by the U. S. Air Force Laboratory Graduate Fellowship Program.

6 References

[1] Puig-Suari, J., and Longuski, J.M., "Modeling and Analysis of Orbiting Tethers in an Atmosphere," *Acta Astronautica*, Vol. 25, No. 11, November 1991, pp. 679-686.

[2] Longuski, J.M., Puig-Suari, J., and Mechalas, J., "Aerobraking Tethers for the Exploration of the Solar System," to appear in *Acta Astronautica*. Also, *43rd IAF Congress*, IAF-92-0001, World Space Congress, Washington, DC, August-September 1992.

[3] Longuski, J.M., Puig-Suari, J., Tsiotras, P., and Tragesser, S.G., "Optimal Mass for Aerobraking Tethers," *44th IAF Congress*, IAF-93-A.2.13, Graz, Austria, October 1993.

[4] Puig-Suari, J., "Aerobraking Tethers for the Exploration of the Solar System," Ph.D. Thesis, School of Aeronautics and Astronautics, Purdue University, 1993.

[5] Puig-Suari, J., Longuski, J.M., and Tragesser, S.G., "A Three Dimensional Hinged-Rod Model for Flexible-Elastic Aerobraking Tethers," *AAS/AIAA Astrodynamics Conference*, AAS-93-730, Victoria, B.C., Canada, August 1993.

[6] Puig-Suari, J., and Longuski, J.M., "Analysis of Aerocapture with Tethers," *AAS/AIAA Astrodynamics Conference*, AAS-91-549, Durango, Colorado, August 1991.